ACS OMEGA

Article

Cite This: ACS Omega 2019, 4, 21931−21944

http://pubs.acs.org/journal/acsodf

Mg−Phenolic Network Strategy for Enhancing Corrosion Resistance and Osteocompatibility of Degradable Magnesium Alloys

Mohammad Asgari,[†,§] Ying Yang,[†,‡,§] Shuang Yang,[∥] Zhentao Yu,[⊥] Prasad K. D. V. Yarlagadda,[†,§] Yin Xiao,*[,†,‡,§,∥] and Zhiyong Li*[,†,§]

[†]The Institute of Health and Biomedical Innovation and [‡]The Australia-China Centre for Tissue Engineering and Regenerative Medicine (ACCTERM), Queensland University of Technology, Brisbane, Queensland 4059, Australia

[§]School of Chemistry, Physics & Mechanical Engineering, Science & Engineering Faculty, Queensland University of Technology, Brisbane, Queensland 4000, Australia

[∥]Key Laboratory of Oral Medicine, Guangzhou Institute of Oral Disease, Stomatology Hospital of Guangzhou Medical University, Guangzhou, Guangdong 510140, China

[⊥]Shaanxi Key Laboratory of Biomedical Metal Materials, Northwest Institute for Non-ferrous Metal Research, Xi'an 710016, China

Supporting Information

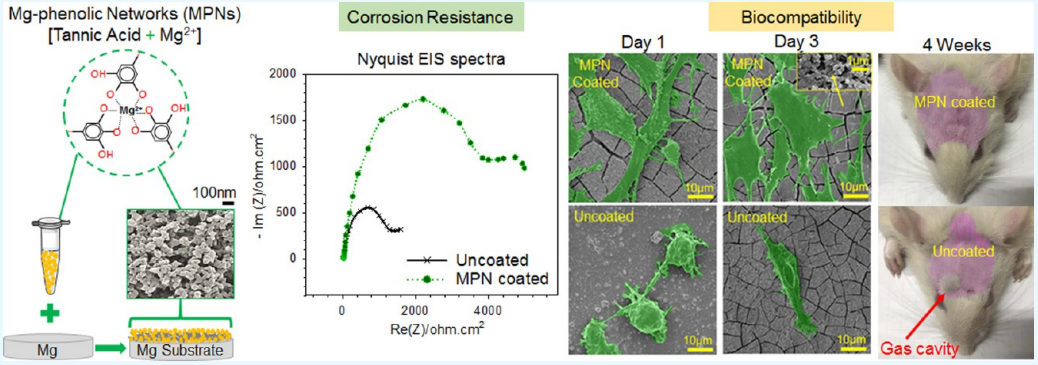

ABSTRACT: Magnesium-based alloys are the most widely used materials for degradable metallic implants and have considerable potential for bone applications owing to their excellent stimulating effect on osteogenesis. However, their high corrosion rate limits their structural stability and causes oxygen deficiency and an excessive increase in the pH around the defect area during bone healing. Magnesium oxides, which are the main corrosion products of Mg, are nontoxic materials with useful effects on new bone formation and pH neutralization. Metal−phenolic networks were introduced recently as a cost-effective and efficient surface modifier and were fabricated by deposition of nanosized metal oxides on different types of substrates using the chemical reaction between phenolic groups and metallic ions. In this study, magnesium oxide films were formed successfully on a Mg-based substrate using Mg−phenolic networks. The effects of various coating parameters on the surface morphology, corrosion resistance, degradation behavior, wettability, and osteocompatibility of degradable metallic materials after surface modification with Mg−phenolic networks were thoroughly investigated for the first time. The results showed that the initial concentration of Mg ions was the main parameter affecting the corrosion resistance, which was almost as much as 3 times that of uncoated samples. Additionally, cytotoxicity and viability assessment and observation of the morphological changes in bonelike cells showed that the in vitro osteocompatibility was significantly enhanced by coatings with Mg concentrations of 2.4−3.6 mg mL^{-1}. Finally, in vivo animal studies using the rat calvarial defect model confirmed that the proposed coating method mitigated the formation of gas cavities around the implantation area by reducing the corrosion rate of the Mg-based implant. The nanosized metal oxides produced by the Mg−phenolic network significantly improved the biodegradability and osteocompatibility of Mg alloys, suggesting a potential approach to advancing the clinical application of Mg alloys.

1. INTRODUCTION

Magnesium-based alloys are the most widely used degradable bone-related implant biomaterials for orthopedic applications.[1−3] In addition to the structural capability of these alloys to provide mechanical stability, Mg contributes to the metabolism of bone regeneration.[4,5] When Mg is implanted in bone defect areas, the contact between the Mg surface and blood plasma (the main component of blood that contains mostly water) results in a chemical reaction (see eq 1[6]). Consequently, Mg ions (Mg^{2+}) are released into the surrounding blood. It has

Received: September 12, 2019
Accepted: November 29, 2019
Published: December 11, 2019

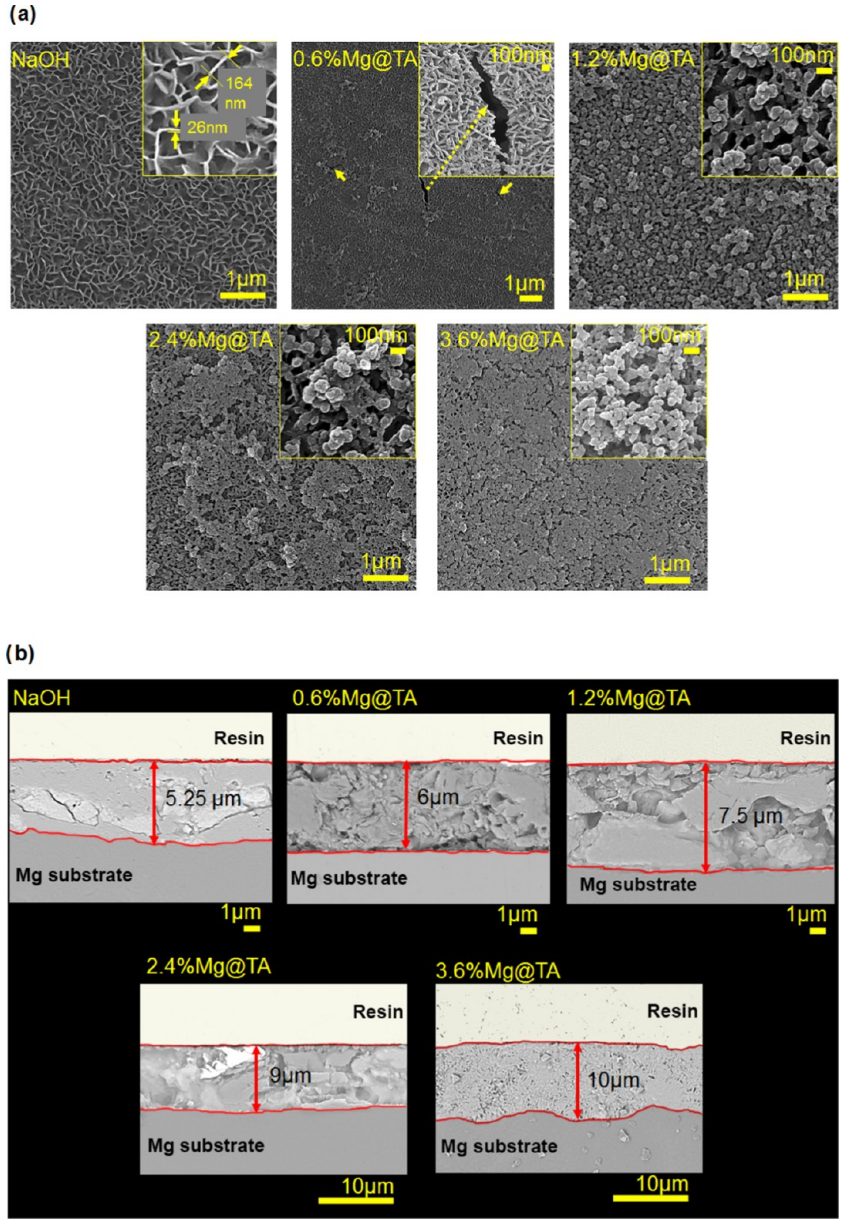

Figure 1. Scanning electron macrographs of (a) surface morphology of the coated samples in different process parameters using a secondary electron detector (SED). (b) Cross section of the coated samples using backscattered electron scanning.

been proved that the Mg ions effectively enhance the proliferation and differentiation of osteogenic stem cells, which can support new bone formation.[7] However, the release dosage of Mg^{2+} ions should be controlled to prevent toxicity to the cells in the implantation area.[8] Most of the released Mg^{2+} ions react with hydroxide ions (OH^-) and form a porous $Mg(OH)_2$ film on the surface of the Mg substrate, which can change to MgO in the absence of water. $Mg(OH)_2$ is relatively insoluble in water and has been used as an inorganic nontoxic medicine for pH neutralization of sour stomach.[9] Additionally, as the main degradation product of magnesium alloys in bone applications, $Mg(OH)_2$ stimulates osteogenesis and reduces osteoporosis, resulting in a mature bone with a higher density.[10,11] Furthermore, it can be applied as an antibacterial agent with a high loading capability.[12]

$$Mg(s) + 2H_2O(aq) \rightarrow Mg(OH)_2(s) + H_2 \uparrow (g) \quad (1)$$

The low standard electrode potential of Mg makes it very reactive in the presence of electrolytes in blood plasma or other aqueous solutions.[13] $Mg(OH)_2$ and/or MgO oxide films are not dense enough to protect Mg-based implants against the high corrosion rate in the physiological environment,[14] which causes an increase in crack initiation and propagation and ultimately decreases the mechanical stability in the defect zone.[1,15] According to eq 1, hydrogen gas (H_2) is another corrosion product resulting from Mg degradation. The flow rate of blood in bone tissues is not naturally high enough to remove the insoluble H_2 bubbles that are released. Therefore, H_2 cavities are formed around Mg implants and prevent the arrival of sufficient oxygen and other necessary nutrients for adhesion, proliferation, and differentiation of bone cells at the implant surface, ultimately killing the cells before bone mineralization begins.[6,16,17] Hence, controlling the high corrosion rate of Mg will reduce the negative consequences of H_2 cavity formation, especially in the days immediately following implantation,

DOI: 10.1021/acsomega.9b02976
ACS Omega 2019, 4, 21931−21944

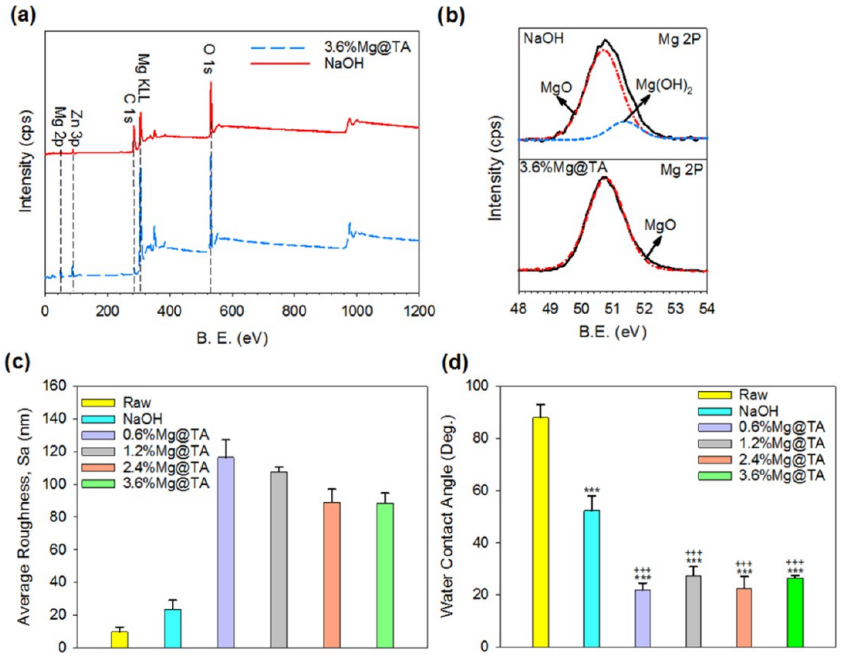

Figure 2. Surface characterization of different samples. X-ray photoelectron spectroscopy (XPS) results: (a) wide scan spectrum, (b) corresponding Mg 2p high-resolution spectrum; (c) average surface roughness (S_a); (d) water contact angle; significance is shown as *** and +++ $p < 0.001$ compared to raw and NaOH samples, respectively.

allowing the nutrient effect of the valuable corrosion products of Mg [i.e., Mg^{2+}, $Mg(OH)_2$] to stimulate bone ingrowth.

Apart from the design of new biocompatible Mg alloys by adding alloying elements such as Zn, Mn, and Ca[18,19] to reduce the corrosion rate of pure Mg, surface modification has been used as the most effective approach to passivate the surface of Mg-based alloys and enhance their corrosion resistance. Biomimetic degradable coatings such as calcium orthophosphate,[14,20] collagen,[21] and biocomposite coatings have been shown to be suitable approaches not only to delay the corrosion of Mg but also to generate a biocompatible interface for bone formation.[22] These strategies prolong the corrosion period by enhancing corrosion resistance of Mg alloy and providing barriers to corrosion electrolyte.[23] Recently, silk fibroin (SF) coating endowed Mg alloys with superior biocompatibility and significantly enhanced corrosion resistance as evidenced by a rabbit spine test for 180 days.[24] SF could also be composited with K_3PO_4 to form a self-healing coating on Mg alloys with pH sensitivity, preferable corrosion resistance, and osteogenic activity.[23] However, the main drawback of these surface passivation methods is that the positive role of Mg oxides in bone mineralization becomes negligible. Therefore, deposition of $Mg(OH)_2$ and MgO coatings by various methods such as ion beam deposition,[25] physical vapor deposition,[26] anodization,[27] and pulse direct current (DC) magnetron sputtering[28] has been proposed to protect Mg alloys. However, most of these methods require special and expensive equipment to deposit Mg oxides on the Mg-based substrate. Furthermore, some of them can be applied only to substrates with simple geometries. Therefore, a cost-effective, simple, flexible, and efficient method to coat Mg-based substrates with Mg oxides could offer significant advantages over the methods mentioned above.

Metal−phenolic networks (MPNs) were recently introduced as a flexible and cost-effective surface modification method for deposition of multiple types of nanoscale biointerfaces on various substrates.[29] MPNs are generally formed by dynamic chemical reactions between metal ions and phenolic molecules using tannic acid (TA) or phytic acid, which are the two main natural polyphenol products.[30,31] Chen et al.[32] proposed a Mg-ion-integrated phytic acid coating to form three-dimensional (3D) networks of Mg oxides. They found that a bonelike structure formed on the Mg substrate, which can effectively improve the corrosion resistance and osteocompatibility, simultaneously stimulating the bioactivity of bonelike apatite precipitation and osteoblast cell adhesion and proliferation in vitro. Although some studies have investigated MPNs as surface coatings on Mg alloys,[33,34] the effects of experimental parameters such as the type and concentration of the Mg ion source and phenolic molecules, the number of coating cycles, and the characteristics of the intermediate layer on the morphology, density, homogeneity, and stability of the deposited film are not fully understood. Furthermore, the effects of those parameters on the degradation behavior, release of Mg ions, corrosion resistance, cytotoxicity, and cell differentiation need to be elucidated to obtain an osteocompatible surface.

In this research, Mg−phenolic networks were deposited on a Mg−Zn alloy and the effects of coating variables such as the concentration of Mg ions and number of coating cycles on the surface morphology and characteristics, corrosion resistance, biodegradability (i.e., ion release), and cytotoxicity were studied to identify the optimal coating parameters for surface passivation of Mg-based implants. Finally, samples were fabricated using the optimal coating parameters and in vivo animal studies were conducted to compare their degradation behavior with that of uncoated (raw) samples.

2. RESULTS AND DISCUSSION

2.1. Characterization of Mg−Phenolic Networks.

2.1.1. Surface Morphology. The surface morphologies of the coated samples after the coating processes are presented in Figure 1a. The initial step of the coating process using the

DOI: 10.1021/acsomega.9b02976
ACS Omega 2019, 4, 21931−21944

NaOH solution produced a uniform nanosized porous film with tiny scales on the surface. The effect of Mg concentration on the morphology after three coating cycles is obvious. The tiny scales on the intermediate layer of step 1 were successfully thickened at the lowest Mg concentration (0.6%). The tiny scales formed in step 1 acted as an intermediate passivation layer that reduced Mg substrate corrosion by allowing Mg ions to react with TA to form the 3D phenolic structure. Additionally, the gaps between the tiny scales were almost filled in 0.6%Mg@TA. When the initial concentration of Mg was increased from 0.6 to 1.2%, the gaps in the intermediate layer were completely filled by Mg−phenolic networks. For the 2.4% Mg group, a cauliflower-like structure was formed and ultimately became connected to form a uniform secondary layer as the concentration increased to 3.6%. Moreover, the image to 0.6%Mg@TA sample shows the formation of cracks on the surfaces of the coated samples after three cycles of coating at this concentration. The micro- and nanocracks indicated release of Mg ions from the substrate and subsequent corrosion. This result indicated that Mg ions at the initial concentration of 0.6% did not react with the free oxygen ions of TA. The remaining oxygen ions would react with the substrate, resulting in a lack of Mg ions and fewer Mg−phenolic networks. Figure 1b compares the thickness of the coating layer in different samples using backscattered electron (BSE) imaging. There was no significant difference between the NaOH- and 0.6%Mg@TA-coated samples. Moreover, the thickness of the coating layer was increased from 6 to 7.5, 9, and 10 μm by increasing the initial concentration of Mg during step 2 of the coating process from 0.6 to 1.2, 2.4, and 3.6%, respectively.

Figure S1a,b illustrates the effect of cycle number on the coating morphology of the 3.6% Mg sample. The thin scales resulting from step 1 were filled after the first cycle (Figure 1a); they were further thickened by Mg phenols and became denser at the end of cycle two. Figure S1b shows that the cauliflower-like networks and then began to appear. Thus, step 2 of the coating process led to filling and thickening of the intermediate layer, initiation of the formation of the 3D Mg−phenolic structure, and the further formation of a uniform, dense coating.

2.1.2. Chemical Composition Analysis of the Mg−Phenolic Film. Figure 2a shows the chemical composition of the NaOH- and 3.6%Mg@TA-coated samples, as representative of the results of steps 1 and 2 of the coating procedure (Figure 1o). C, O, Mg, and Zn were present in both coatings. Figure 2b shows the high-resolution Mg 2p spectra of the coating after steps 1 and 2. The Mg 2p spectra of the NaOH sample showed that step 1 introduced a mixture of MgO and $Mg(OH)_2$. In contrast, MgO was the main component of the 3.6%Mg@TA sample owing to the chemical reaction between free O^{2-} ions from TA and Mg^{2+} ions, which led to the formation of cauliflower-like Mg−phenolic networks.

2.1.3. Surface Roughness. Figure 2c summarizes the average roughness (S_a) of various samples observed by atomic force microscopy (AFM) in a scanning range of 20 × 20 μm^2. The average S_a value was approximately 10 nm for the polished raw samples and increased to 23 nm after step 1 of coating. The roughness of the samples completely coated with Mg−phenolic networks increased to 88, 90, 107, and 116 nm for the 3.6%Mg@TA, 2.4%Mg@TA, 1.2%Mg@TA, and 0.6%Mg@TA samples, respectively. The roughness values of the 2.4%Mg@TA and 3.6%Mg@TA samples were quite similar. Moreover, the surface roughness decreased as the initial concentration of Mg increased owing to smoothing at higher concentrations.

2.1.4. Wettability. The results of wettability assessment are shown in Figure 2d. The average water contact angle of the raw samples was ∼88°. The NaOH coating decreased the water contact angle by 41% compared to that of the raw samples ($p < 0.001$). It is also clear that regardless of the initial Mg concentration, the addition of Mg−phenolic networks enhanced the hydrophilicity. Hydrophilic surfaces with water contact angles of 20−40° can reportedly provide the highest levels of cell attachment.[35−38] As shown in Figure 2d, all of the coated samples exhibited moderate water contact angles of 21−27°, which were significantly different from that of the raw sample ($p < 0.001$). Furthermore, the deposited Mg−phenol networks also significantly increased the hydrophilicity compared to that of the NaOH coating ($p < 0.001$).

2.2. Corrosion Resistance Analysis. Figure 3a,b shows the electrochemical impedance spectroscopy (EIS) and potentiodynamic polarization (PDP) curves. The Nyquist impedance spectra clearly show the kinetics of electrochemical corrosion of the samples. Figure 3c shows the corresponding equivalent circuit for the coated samples,[39−41] where R_s, Q_{dl}, R_{ct}, Q_p, and R_p represent the solution resistance, double-layer capacitance, reaction resistance associated with the interfacial charge-transfer reaction, coating capacitance, and coating resistance, respectively. For the raw sample, R_{ct}, Q_p, and R_p were ignored. Using the equivalent circuit and obtained EIS curves, curve fitting

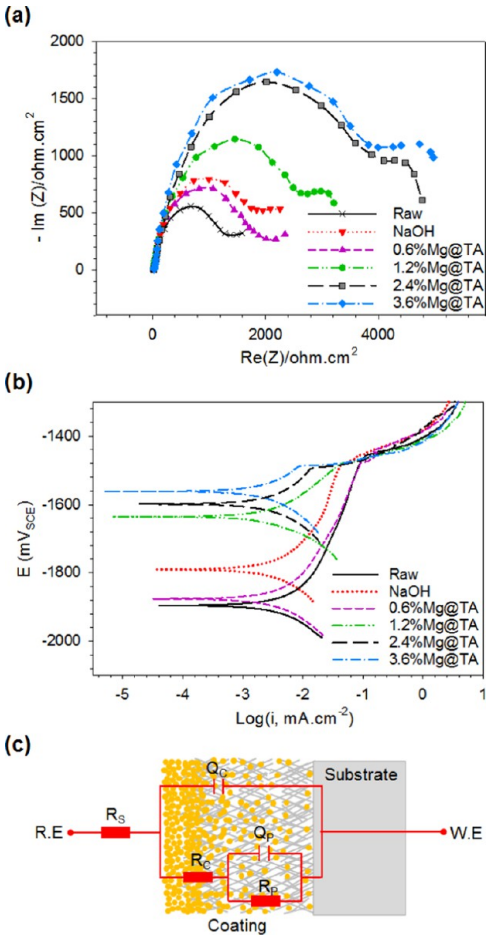

Figure 3. Comparison between electrochemical behavior of different samples: (a) Nyquist EIS spectra and (b) PDP curves. (c) Equivalent circuit model used to interpretation of the corrosion behavior of the coated samples.

DOI: 10.1021/acsomega.9b02976
ACS Omega 2019, 4, 21931−21944

Table 1. Corresponding Parameters Determined from Curve Fitting of the EIS and PDP Results

	Nyquist EIS spectra					polarization curves	
samples	R_s (Ω cm^2)	Q_{dl} (μF cm^{-2} s^{n-1})	R_{ct} (kΩ cm^2)	Q_p (μF cm^{-2} s^{n-1})	R_p (kΩ cm^2)	E_{corr} (mV$_{SCE}$)	I_{corr} (μA cm^{-2})
raw	22.0	71.1	1.619			−1896	5.616
NaOH	32.5	19.9	2.042	629	1.235	−1790	4.046
0.6%Mg@TA	19.8	18.3	1.860	1371	0.537	−1876	5.186
1.2%Mg@TA	16.4	13.9	2.893	961	1.056	−1589	2.190
2.4%Mg@TA	23.7	13.7	4.543	1074	0.903	−1598	1.205
3.6%Mg@TA	30.3	14.5	4.549	1039	0.942	−1561	1.191

analysis was performed using EC-Lab software; the corresponding data for each element of the circuit were extracted and are summarized in Table 1. R_{ct} is known to have the largest effect on the impedance of the corrosion reaction.[32] As shown in Table 1, the R_{ct} value of the 0.6%Mg@TA sample was even lower than that after the first step of coating (i.e., coating with NaOH), possibly owing to cracking during the coating process (Figure 1). The increase in the Mg concentration caused an increase in R_{ct}. Therefore, it can be concluded that the porous coating of Mg−phenolic networks with the optimal Mg concentration can significantly enhance the corrosion resistance of Mg-based alloys. The obtained curves from PDP tests (Figure 3b) and the corresponding values for the E_{corr} and I_{corr} extracted from the polarization curves using the Tafel method (Table 1) had almost the same trend as that of EIS curves (Figure 3a) and the R_{ct} value among the considered samples (Table 1). The 2.4%Mg@TA and 3.6%Mg@TA samples delivered the lowest value for the corrosion current density (I_{corr}) among all of the samples (Table 1). The value of the I_{corr} for these samples is almost 5 times lower than that of the raw sample. As far as I_{corr} is directly proportional to the corrosion activities,[42] we can claim that the Mg−phenolic networks with a proper coating procedure deliver proper electrochemical stability and promote anticorrosion performance of the Mg-based substrate kinetically. Moreover, the free corrosion potential (E_{corr}) of the coated samples shifted toward the more positive potentials, indicating the thermodynamic reaction activity of the coated samples in phosphate-buffered saline (PBS) was more suppressed compared to that of the uncoated sample.[42]

Taken together, all of these results can be considered as convincing evidence to prove that performing Mg−phenolic network strategy with a proper initial Mg concentration during the coating procedure can serve a proper corrosion protection for the Mg-based substrate. Furthermore, the R_{ct} and I_{corr} values of the 2.4%Mg@TA and 3.6%Mg@TA samples were all almost similar (Table 1), indicating that initial Mg concentrations exceeding 2.4% would not further improve corrosion resistance.

2.3. Degradation Behavior. Figure 4a,b shows the Mg concentration and the volume of H_2 gas evolution within 3 weeks and at five time points during immersion of the samples in PBS solution at 37 ± 0.5 °C, respectively. The raw sample clearly released the highest quantity of Mg ions and hydrogen evolution, indicating that it had the highest degradation rate. With increasing initial Mg concentration in the coating procedure, the degradation rate decreased that led to less release of Mg ions and hydrogen evolution. Additionally, for all of the samples, the Mg concentration in the extracted solution increased dramatically from day 1 to day 3 and then gradually increased from day 3 to day 7. The reason may be the formation of insoluble salty clusters on the sample surfaces, which decreased after the surface area was exposed to the solution.[43] It is worth mentioning that the trend of changing in the quantity of the measured hydrogen evolution (Figure 4b) are in agreement with that of the Mg concentration (Figure 4a) in all of the considered time points.

Figure 4c shows the pH of the collected PBS solution after immersion of the samples. The differences in the degradation rates of the samples resulted in differences in the hydroxide ion (OH^-) release and pH.[4] The pH for the raw and 0.6%Mg@TA samples reached 8.75 owing to the absence of a suitable passivation layer for the raw sample and cracking that occurred during coating of the 0.6%Mg@TA sample. The NaOH-treated and 1.2%Mg@TA samples produced moderate increases in pH to 8.70 and 8.74, whereas the 2.4%Mg and 3.6%Mg samples caused the smallest pH changes, to 8.34 and 8.40, respectively, on day 1. As the immersion time increased to 3 days, the pH of all of the samples increased. When the immersion time increased to 7 days, a temporary hydroxide passivation layer that was thermodynamically stable at pH values above 8.3 may have formed (Figure 4d).[43] This layer caused the degradation rate to increase more slowly and protected against significant changes in the pH, especially for the raw sample. Figure 4d shows the surface morphology of the samples after 7 days of immersion in PBS. Although a more slatelike structure formed on the surface of the raw sample, it still had a larger contact area than the coated samples owing to severe cracking. Figure 4e shows the EDX profiles of the insoluble cluster shown in Figure 4d. Despite the formation of cracks with submicron widths, the Mg−phenolic films with different initial Mg concentrations were quite stable and decreased the corrosion rate, especially for the 1.2%Mg@TA, 2.4%Mg@TA, and 3.6%Mg@TA samples. Even the NaOH-treated sample maintained its nanoscale porous coating on day 7 (Figure 4d). After day 7, the samples exhibited different degradation rates. The Mg ion release of the raw sample continued to increase, but the amount of release tended to be steady at days 15 and 21. For the NaOH-treated sample, the release of Mg ions increased more slowly, indicating better corrosion resistance compared to the raw sample. For the samples coated with the Mg−phenolic networks, the degradation rate decreased from day 7 to day 21. Figure 4e shows the EDX profiles of these hydroxide films. However, the presence of dissolved chloride ions (Cl^-) at high concentrations in the PBS solution, which mimicked that of blood plasma,[44] would accelerate the corrosion rate of Mg and convert some of the temporary hydroxide coating into soluble $MgCl_2$, further increasing the exposed area.[14] At high pH values, formation and dissolution of the hydroxide layer are typically competing processes. Free Cl^- ions played a prominent role in the increase in pH. Furthermore, the cracks on the substrate released more Mg ions and thus increased the pH to 9.23, 9.22, 9.24, 9.11, 9.06, and 9.0.3 for the raw, NaOH, 0.6%Mg@TA 1.2%Mg@TA, 2.4% Mg@TA, and 3.6%Mg@TA samples, respectively. The pH of the raw samples reached 9.36 at day 15, whereas the pH of the modified samples decreased compared to that on day 7.

DOI: 10.1021/acsomega.9b02976
ACS Omega 2019, 4, 21931−21944

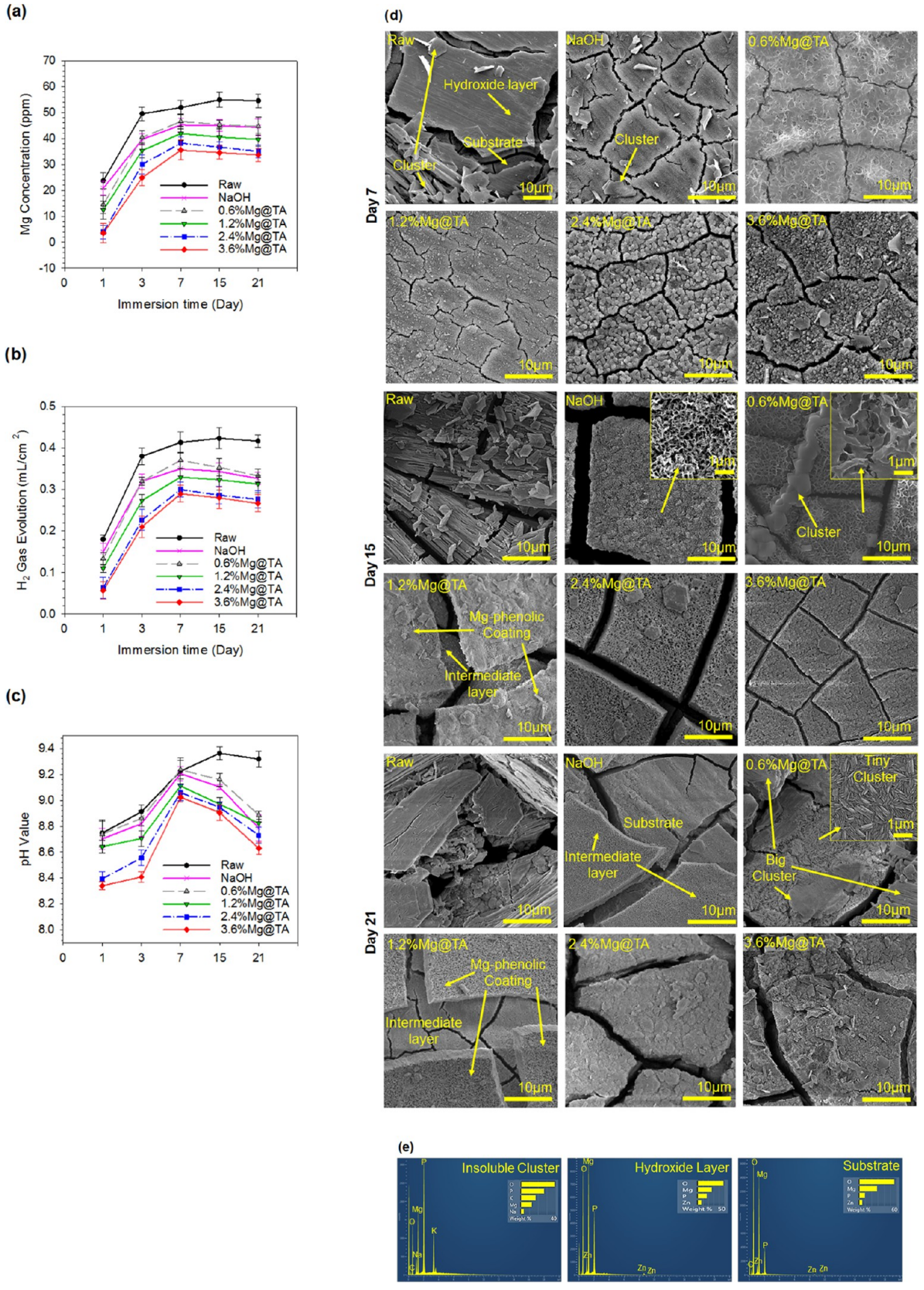

Figure 4. Variation of four different parameters during 3 weeks degradation of different samples in PBS solution at 37 ± 0.5 °C: (a) concentration of released Mg element, (b) hydrogen gas evolution, (c) pH value, (d) surface morphology; (e) energy-dispersive X-ray (EDX) spectrum and weight% elemental quantitative data representative of the insoluble cluster, the hydroxide layer, and substrate fragments.

Insoluble salty clusters formed on the surface of the raw sample. Despite the cracking, the coating layer was present and connected to the substrate of the 2.4%Mg@TA and 3.6% Mg@TA samples. In contrast, the Mg−phenolic networks were

DOI: 10.1021/acsomega.9b02976
ACS Omega 2019, 4, 21931−21944

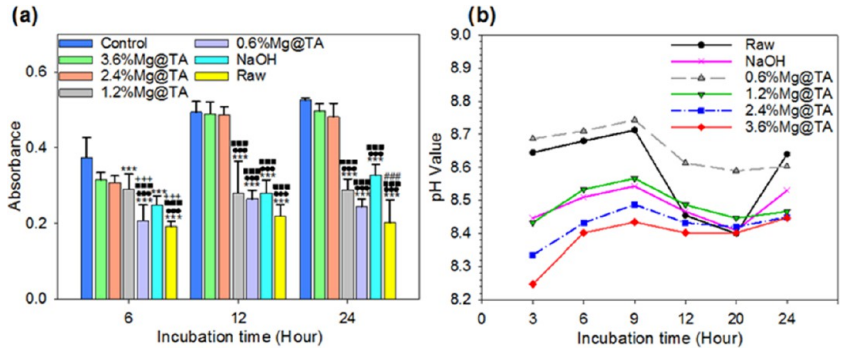

Figure 5. (a) Average absorbance of MC3T3-E1 cells seeded on different samples after 6, 12, and 24 h.***, ●●●, ■■■, $^{+++}$, and $^{\#\#\#}$ $p < 0.001$, differences from the control group, 3.6%Mg@TA, 2.4%Mg@TA, 1.2%Mg@TA, and NaOH at each time point, respectively. (b) pH value changes of the culture media during 24 h incubation of MC3T3-E1 cells with different samples.

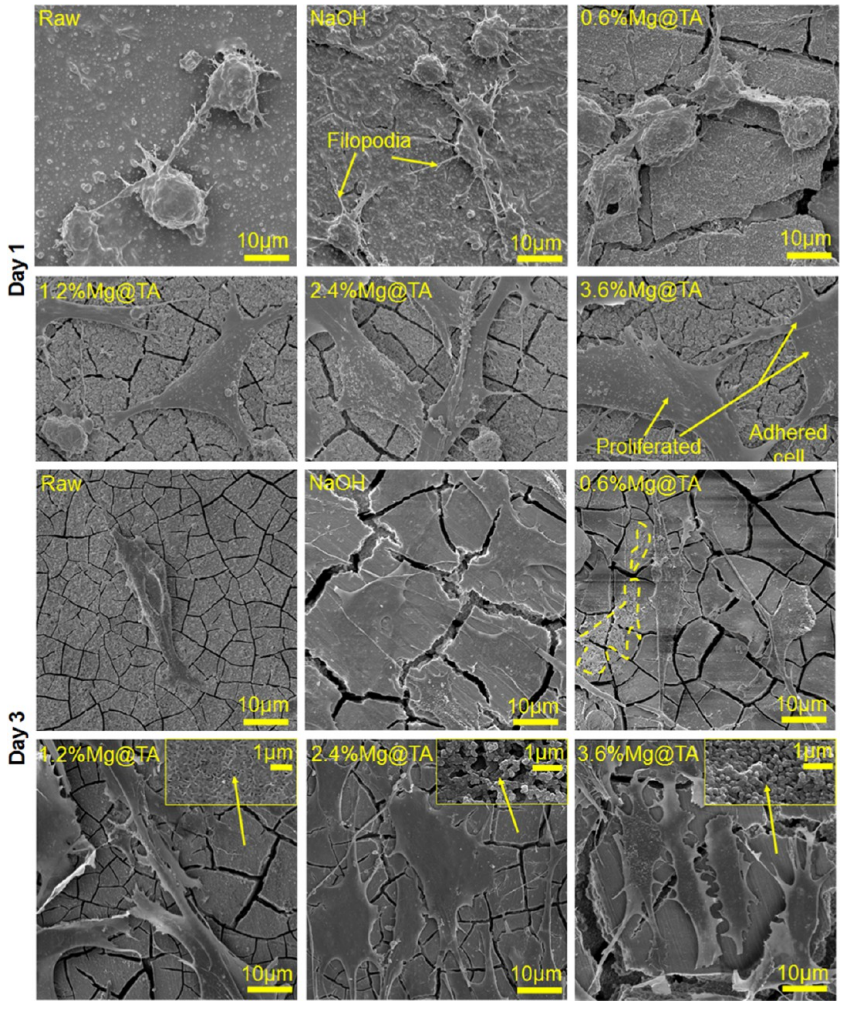

Figure 6. SEM images of the morphology of MC3TC-E1 cells cultured on different samples at day 1 and day 3 of incubation.

separated from the intermediate layer of the 1.2%Mg@TA samples. A uniform porous oxidized layer was formed on the surface of the 0.6%Mg@TA and NaOH-treated samples. However, the 0.6%Mg@TA sample was more severely corroded than the NaOH sample owing to its highly porous surface. This result indicates that the Mg−phenolic coating was not stable enough to passivate the substrate at day 15.

The cracks on the surfaces of all of the samples were wider on day 21 (Figure 4d), and more phosphate-based cluster structures had formed. The 2.4%Mg@TA and 3.6%Mg@TA samples still had stable Mg−phenolic networks. In the 1.2% Mg@TA samples, the Mg−phenolic networks had begun to peel off from the intermediate layer. The tiny and large clusters of the 0.6%Mg@TA samples decreased the corrosion activity. The NaOH-treated samples were divided into coated and uncoated areas as the intermediate coating layer was removed from the Mg substrate. As on days 7 and 15, the morphology of the raw sample consisted of the oxidized substrate and cluster structure. The pH of all of the samples on day 21 was lower than that on day 15 owing to the precipitation of more insoluble salty clusters

DOI: 10.1021/acsomega.9b02976
ACS Omega 2019, 4, 21931−21944

containing phosphate on the surface of the samples resulting from the high concentration of phosphate in the PBS solution.[43] Furthermore, part of the Mg−phenolic passivation film was still present on the 2.4%Mg@TA and 3.6%Mg@TA samples.

Overall, the changes in Mg ion release, H_2 gas evolution, and pH were clearly consistent. In light of the surface morphology, the intermediate and Mg−phenolic layers as well as the formation of insoluble phosphate-based clusters were the main factors affecting the degradation behavior.

2.4. In Vitro Osteocompatibility Assessment.

2.4.1. Short-Term Cytotoxicity Assessment. Figure 5a summarizes the results of short-term cytotoxicity assessment of the MC3T3-E1 cells using 3-(4,5-dimethylthiazol-2-yl)-2,5-diphenyltetrazolium bromide (MTT) assay after 6, 12, and 24 h. Among all of the groups, the 2.4%Mg@TA and 3.6%Mg@TA samples showed an acceptable level of viability during the first 24 h of incubation of the bonelike cells, indicating that they provide a suitable physiological ambient for stimulating cell adhesion and proliferation. Figure 5b shows the pH values of the culture media containing MC3T3-E1 cells added to the samples during 24 h. The initial pH value of the control group (i.e., the clear medium with cells only) was 7.77 and varied between 7.78 and 7.92 during that time period. The 2.4%Mg@TA and 3.6%Mg@TA samples clearly caused the least fluctuation in the pH of the culture medium, and the corrosion rate was stable. Culture media with alkaline pH values of 8.40−8.50 support the highest osteoblast viability in vitro.[45−47] The average pH values of the 2.4%Mg@TA and 3.6%Mg@TA samples during the first day of cell culture were 8.42 and 8.39, respectively.

2.4.2. Morphology Assessment of MC3TC-E1 Cells. The morphological changes in the seeded MC3T3-E1 cells on the samples were investigated using scanning electron microscopy (SEM) imaging to compare the effects of the Mg−phenolic coating on the adhesion and proliferation of the bonelike cells.

Figure 6 presents SEM micrographs showing the morphology of MC3T3-E1 cells cultured on the samples at the end days 1 and 3. On day 1, the 3.6%Mg@TA, 2.4%Mg@TA, and 1.2% Mg@TA samples showed high osteocompatibility, with cell attachment and suitable spreading owing to the stable moderately alkaline pH and suitable surface wettability of the protective coating.

On day 3, the morphology of cells cultured on the samples indicated cell proliferation. A few cells became attached to the raw and 0.6%Mg@TA samples, indicating that they could not provide a suitable biocompatible physiological environment for cell proliferation. In contrast, the 3.6%Mg@TA, 2.4%Mg@TA, 1.2%Mg@TA, and NaOH-treated samples exhibited improved biocompatibility, with more cells and acceptable levels of proliferation. Specifically, the 3.6%Mg@TA and 2.4%Mg@TA samples showed the best osteocompatibility among all of the groups. The above results were consistent with the short-term cytotoxicity assessment (Section 2.4.1), wettability results (Section 2.1.4), and corrosion resistance experiment (Section 2.2). That is, the 3.6%Mg@TA and 2.4%Mg@TA samples with the proposed porous osteocompatible Mg−phenolic networks exhibited acceptable corrosion resistance by mitigating the negative effect of excessive release of H_2 bubbles and exhibited suitable wettability for adhesion and proliferation of bonelike cells.

2.4.3. Indirect Viability Assessment. Surface properties such as roughness and wettability, the pH of the culture medium, the concentration of Mg ions, and oxygen deficiency due to the release of H_2 gas bubbles can be considered to be the four main parameters directly affecting the in vitro viability, in particular, the medium-term cytocompatibility, of the Mg alloys. Indirect viability assessment is a common method of evaluating the in vitro medium-term osteoblastic cytocompatibility of such alloys and their capacity to mitigate the effects of these surface properties, increase of pH, and H_2 gas evolution. That is, indirect viability assessment can provide better information about the medium-term influence of the degradation of Mg-based alloys on the surrounding physiological environment in vitro. Therefore, to focus on the effect of the release of Mg^{2+} ions on the viability of osteoblast-like cells, indirect viability assessment of extracted media mixed with 1× Dulbecco's modified Eagle's medium (DMEM) at a 1:1 ratio was performed. The average pH values of the media collected from the 3.6%Mg@TA, 2.4%Mg@TA, 1.2%Mg@TA, 0.6%Mg@TA, NaOH-treated, and raw samples were 8.12, 8.18, 8.25, 8.39, 8.30, and 8.41, respectively. Figure 7 shows the results of the MTT assay after 1 and 3 days of

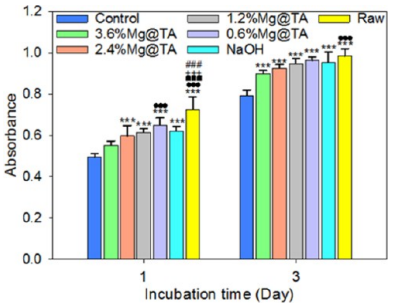

Figure 7. Average absorbance of MC3T3-E1 cells after 1 and 3 days incubation with different culture media. ***, ●●●, ■■■, $^{+++}$, and $^{###}$ $p <$ 0.001, differences from the control group, 3.6%Mg@TA, 2.4%Mg@TA, 1.2%Mg@TA, and NaOH at each time point, respectively.

cell culture with the prepared culture medium for each group. The absorbance of all of the samples obviously differed significantly from that of the control group ($p < 0.001$) on day 1. This finding confirms the stimulating effect of Mg corrosion products (especially Mg^{2+} ions) on the proliferation of bonelike cells reported by Wu et al.[7] Furthermore, Galow et al.[46] have reported that culture media with alkaline pH enhance the viability of osteoblast-like cells in vitro. They claimed that higher pH values of up to 8.4 cause the higher viability.

Figure 8 shows confocal images of the morphology of the cultured MC3T3-E1 cells in the media extracted on day 1. Among all of the groups, the highest numbers of adhered and proliferated cells were observed on the raw and 0.6%Mg@TA samples, which is consistent with the MTT results (Figure 7). On day 3, the same trend as day 1 was observed for MTT results. There was still a significant difference between the control group and the other groups ($p < 0.001$). The increase in the absorbance of all of the groups from day 1 to day 3 indicates enhancement of the proliferation mechanisms of the cells. The confocal images of the cells on day 3 are shown in Figure 9. The cells clearly proliferated well. The differences in cell proliferation among the groups can be explained in terms of the difference in the medium pH.

In summary, the indirect viability test showed that the dose of Mg ions from uncoated Mg-based alloys (i.e., the raw sample) resulted in an alkaline pH in vitro, enhancing proliferation. Furthermore, the 3.6%Mg@TA and 2.4%Mg@TA samples have not only an effective coating of Mg−phenolic networks and the most osteocompatible surface among all the groups, which

DOI: 10.1021/acsomega.9b02976
ACS Omega 2019, 4, 21931−21944

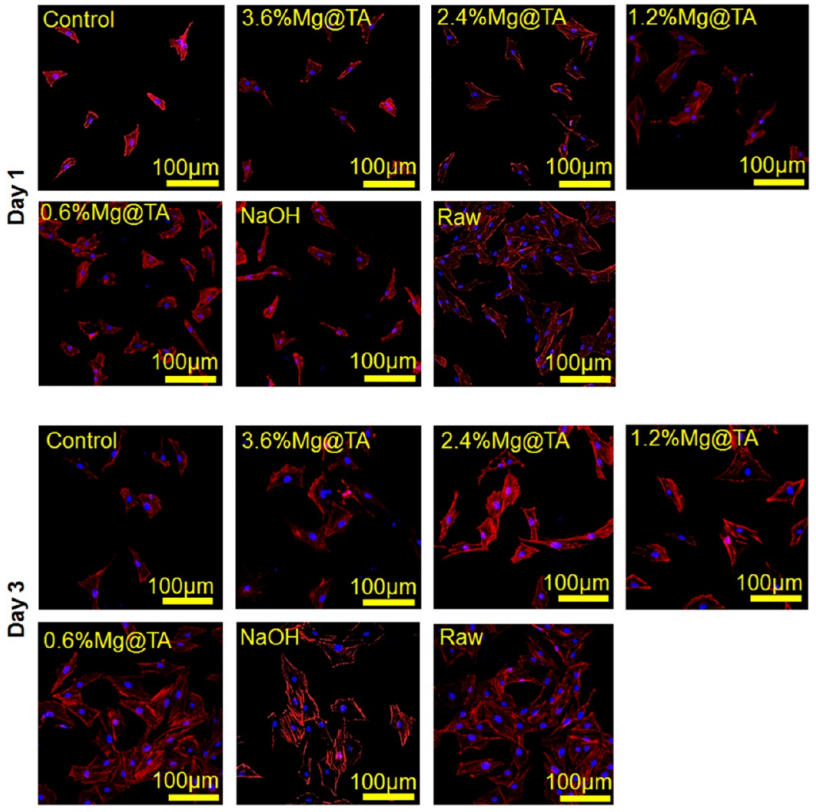

Figure 8. Confocal images of the cytoskeletal arrangement of MC3TC-E1 cells incubated with different culture media at days 1 and 3.

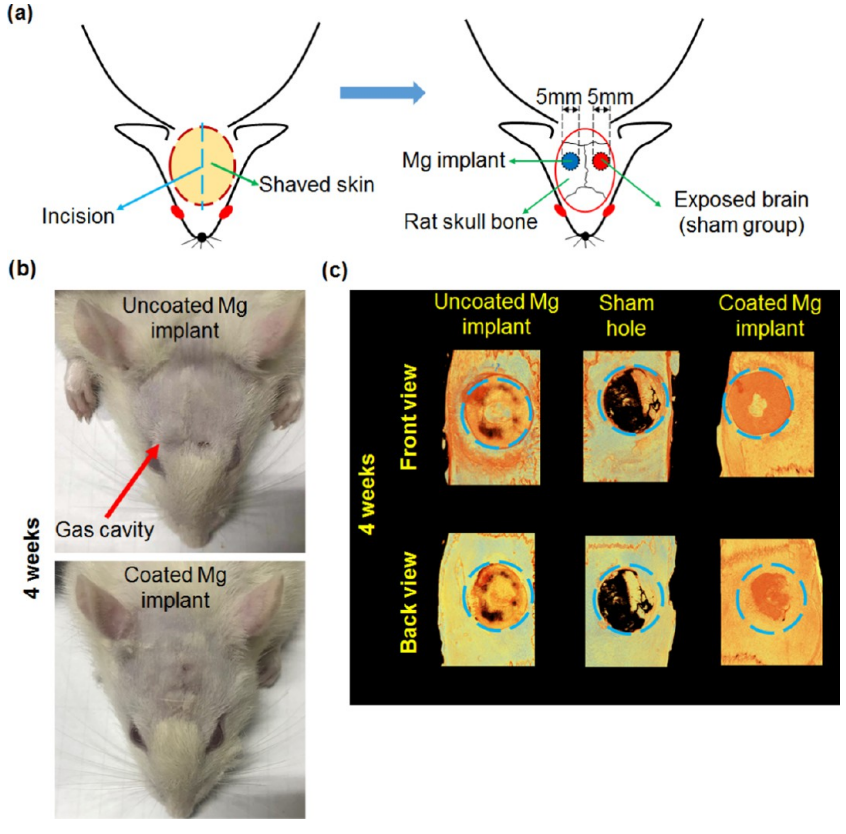

Figure 9. (a) Schematic of the conducted rat cranial bone defect surgery. Two 5 mm diameter critical-sized defects were made on the skull; (b) comparison between uncoated and coated Mg implants in terms of the formation of subcutaneous hydrogen gas cavity in the implantation area; (c) front and back views of the reconstructed microcomputed tomography (μCT) images obtained at 4 weeks after implantation surgery. The blue circle indicates the initial size of the defects.

DOI: 10.1021/acsomega.9b02976
ACS Omega 2019, 4, 21931−21944

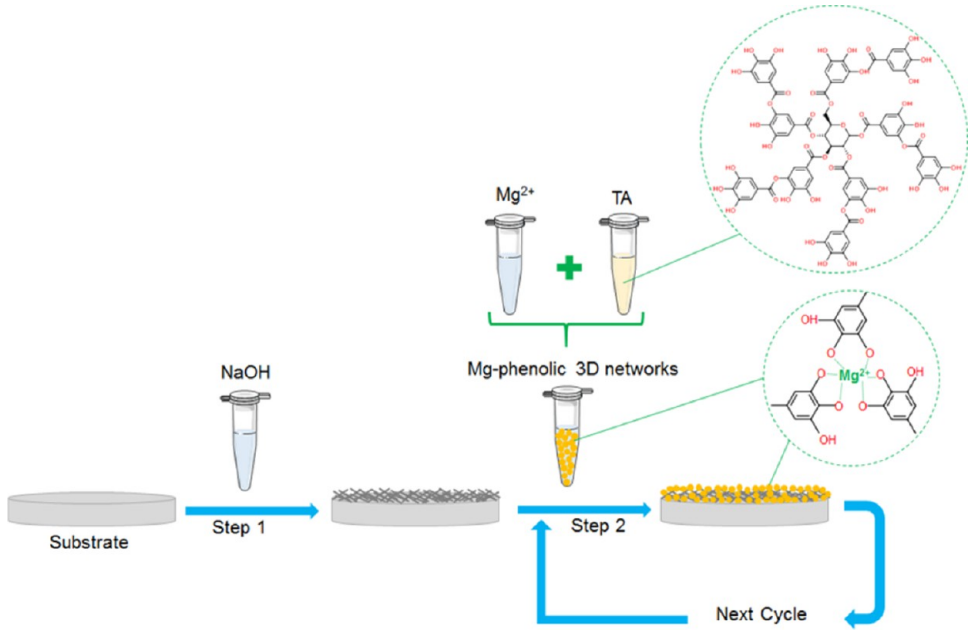

Figure 10. Schematic of the assembly of Mg−phenolic networks on Mg-based alloys.

results in reduced cytotoxicity, but also can still release corrosion products, improving the viability of the biological fluid in the zone around the implantation area.

2.5. In Vivo Implantation of Mg Disks in Rat. After the implantation surgery according to the procedure describes in Section 4.8.2 (Figure 9a) and during the 4 week period before the final surgery for harvesting the skull bone blocks, all of the rats were in good health and showed wound healing without any severe side effects.

2.5.1. Observation of Subcutaneous Hydrogen Gas Cavity. For Mg-based implants with a higher degradation rate, subcutaneous hydrogen gas cavities can be easily observed in the region around the implantation area.[6,16,17] Regardless of the size of the Mg-based implant, the formation of such cavities can be considered convincing evidence for the high degradation rate and undesirable corrosion resistance, which can limit the biocompatibility of such biomaterials. In previous studies, for example, in Lin et al.,[48] photographs of the shaved skin covering the defects in the calvarial region have been used to compare the degradation behavior of different Mg-based implants. Figure 9b compares the formation of subcutaneous hydrogen gas pockets in the uncoated and coated Mg implants 4 weeks after implantation. An obvious gas cavity formed in the implantation area of the uncoated Mg disk. In contrast, no obvious gas pockets formed near the Mg disks coated with Mg−phenolic networks, indicating that the passivation coating decreased the degradation rate of the Mg implants, allowing sufficient time for blood flow to remove the created hydrogen gas bubbles in the implantation area and prevent accumulation of these bubbles. Preventing or at least mitigating the formation of H_2 gas cavities can increase the oxygen supply to the defect area and improve the biocompatibility of Mg-based implants.

2.5.2. Micro-CT Findings. Figure 9c compares focused front and back views of the reconstructed micro-CT images of defect area with uncoated and coated Mg implants as well as the sham control group obtained 4 weeks after implantation. Regardless of the volume of bone formed around the Mg implant, the difference in the degradation of the uncoated and coated samples is obvious. In the uncoated Mg implant, some localized corrosion pits and/or holes were formed, indicating a higher corrosion rate than that of the implants coated with Mg−phenolic networks, on which there were no obvious voids or holes. The accumulation of hydrogen gas near the uncoated sample can be attributed to these corrosion features (Figure 9b). As the degradation rate increased, the formation of subcutaneous gas pockets became more likely.

3. CONCLUSIONS

In this research, nanostructured Mg−phenolic networks were formed on a Mg-based alloy by dip-coating in a solution containing Mg and phenol groups. The two main goals were to enhance the corrosion resistance and osteocompatibility of Mg-based degradable implant materials. The following results were obtained:

(1) The concentration of Mg ions in the coating solution was found to be the main factor affecting the performance of the coating. The corrosion resistance increased with increasing concentration of Mg ions in the coating solution. The corrosion resistance of the 3.6%Mg@TA and 2.4%Mg@TA samples increased by 180% compared to that of the raw sample.

(2) Observations of the degradation behavior showed that the Mg−phenolic network coating can be quite stable in the first few weeks of immersion in PBS solution.

(3) Direct short-term cytotoxicity assessment indicated that the 3.6%Mg@TA and 2.4%Mg@TA coatings significantly decreased the cytotoxicity of the Mg-based substrate in the first day after implantation.

(4) SEM images of the morphology of osteoblast-like cells showed that the Mg-based substrate with a suitable coating of Mg−phenolic networks had an osteocompatible surface that significantly enhanced cell adhesion and proliferation in the first few days after cell seeding.

(5) Indirect medium-term viability assessment showed that the media extracted from even the samples with the highest Mg concentration in the passivation coating (i.e.,

DOI: 10.1021/acsomega.9b02976
ACS Omega 2019, 4, 21931−21944

3.6%Mg@TA and 2.4%Mg@TA) enhanced the viability of the bonelike cells.

(6) In vivo animal experiments revealed that coating Mg-based implants with appropriate passivation layers containing Mg−phenolic networks can control the degradation rate of the implants and mitigate the formation of subcutaneous hydrogen gas cavities in the implantation area.

Overall, passivation of Mg-based alloys with 3.6%Mg@TA and 2.4%Mg@TA coating solutions produced a surface with excellent osteocompatibility that protected the alloys from severe degradation and prevented the formation of excessive H_2 gas bubbles and the resulting oxygen deficiency. Thus, our coating procedure with Mg−phenolic networks shows promise for widening the application of Mg-based degradable implants for bone regeneration.

4. MATERIALS AND METHODS

4.1. Substrate Preparation. Casted ingots of Mg−2.8%Zn alloy were extruded to billets with a diameter of 10 mm. Then, the samples with a diameter of 6 mm and a thickness of 1 mm were machined from the extruded billets. All of the mentioned fabrication processes were carried out in Shaanxi Key Laboratory of Biomedical Metal Materials of Northwest Institute for Nonferrous Metal Research (Xi'an, China). Afterward, the disks were polished with SiC papers down to 4000 grit. Then, all of the samples were ultrasonically cleaned in 100% acetone (10 min) and 100% ethanol (10 min) and finally rinsed in deionized (DI) water to remove any surface contaminations.[49]

4.2. Mg−Phenolic Network Deposition. The coating procedure is summarized schematically in Figure 10. The Mg−phenolic networks were coated on disk samples in two steps. In the first step, the prepared Mg−2.8%Zn disks were immersed in NaOH with a pH of 10 for 90 min. A uniform nanosized film of Mg oxides [both $Mg(OH)_2$ and MgO] can form on Mg substrates immersed in NaOH solution.[32,50] Then, the samples were dip-coated in a prepared solution containing 1 mg mL^{-1} TA (analytical grade, purity = 99%, Sigma-Aldrich) combined with $MgCl_2$ (analytical grade, purity = 99%, Thermo Fisher Scientific, Australia) at four concentrations (0.6, 1.2, 2.4, and 3.6 mg mL^{-1}) in NaOH solution (pH = 10). After 30 min, the samples were removed and washed 3 times with the NaOH solution to remove any salty liquid from their surfaces. In the second step, this procedure was repeated using a fresh solution to perform the second and third cycles and to form a uniform Mg−polyphenolic network surface. To reduce undesirable oxidation, the coated samples were kept in a vacuum desiccator. The NaOH + 1% TA + 3.6% $MgCl_2$, NaOH + 1% TA + 2.4% $MgCl_2$, NaOH + 1% TA + 1.2% $MgCl_2$, NaOH + 1% TA + 0.6% $MgCl_2$, and NaOH coating solutions and the samples coated with them are denoted 3.6%Mg@TA, 2.4%Mg@TA, 1.2%Mg@TA, 0.6%Mg@TA, and NaOH, respectively.

4.3. Surface Morphology Assessment of the Mg−Phenolic Film. To observe the surface morphology of the coated samples after the coating procedure mentioned in Section 4.2, the samples were coated with a thin layer (∼10 nm) of gold using a sputter (EM SC005 Gold Coater, Leica). Then, the surface morphology of the different samples was observed using scanning electron microscopy (SEM, JEOL 7001F, Japan). A secondary electron detector (SED) was used to capture the detailed shape and surface information. Parallel samples were prepared to observe the cross-sectional view of the coated samples. To that aim, the samples were mounted inside the epoxy resin and after the cutting and polishing procedures the cross section of the samples was coated with a very thin layer (∼4 nm) of platinum using a sputter (EM ACE600 Platinum Coater, Leica). Finally, the cross-sectional view of the coating layer of the different samples was captured using SEM (SEM, JEOL 7001F, Japan). Backscattered electron (BSE) imaging was applied to extract chemical contrast information.

4.4. Surface Characterization of the Mg−Phenolic Film. The chemical composition of the sample surfaces was examined by X-ray photoelectron spectroscopy (XPS) using the XPSpeak 4.1 package to analyze the high-resolution spectra and fit the peaks to bonding states. The wettability of the surfaces was assessed by conducting a simple water contact angle test at room temperature and 50% relative humidity using the sessile-drop method on an inclined plate. The roughness of the samples was quantified by atomic force microscopy (AFM) in a scanning range of 20 × 20 μm^2. Each experiment was repeated at least 3 times for statistical analysis.

4.5. Corrosion Resistance Assessment. The effect of the Mg−phenolic coating on the corrosion resistance was examined by electrochemical impedance spectroscopy (EIS) with an electrochemical unit (VSP, Bio-Logic Science Instruments, France) sample as the working electrode, a saturated calomel electrode as the reference electrode, and a platinum foil as the counter electrode. Phosphate-buffered saline (PBS) solution was used as the electrolyte. The side and bottom surfaces of the disk samples were covered by silicon glue, and only the top surface (28.3 mm^2) was exposed to the electrolyte. All of the tests were performed at 37 ± 0.5 °C. The EIS data were recorded from 200 kHz to 100 mHz with a 10 mV sinusoidal perturbing signal.[33]

Accordingly, the potentiodynamic polarization (PDP) tests were conducted at a scanning rate of 1 mV s^{-1}. Then, the Tafel method with linear extrapolation of the active polarization zone in the cathodic polarization section of PDP curves was applied to extract the current density (I_{corr}) and corrosion potentials (E_{corr}).[32] The EC-Lab software package (V11, Bio-Logic Science Instruments, France) was applied to analyze the EIS and PDP results.

4.6. Degradation Behavior. The degradation behavior was examined by immersing the samples in PBS solution (pH = 7.4) for 3 weeks at 37 °C. The surface/volume ratio was 56 mm^2 mL^{-1}. The time checkpoints were set as day 1, day 3, week 1, week 2, and week 3. The PBS solutions were refreshed every 2 days with 500 μL of a fresh solution using a method similar to that mentioned in refs 51 and 52. At the end of each interval, the concentration of Mg^{2+} ions released into the extracted PBS solution was determined using inductively coupled plasma optical emission spectroscopy (ICP-OES 700, Agilent) after measuring the pH value of the extracted using a pH meter (Thermo Fisher Scientific) in each time checkpoints. Parallely, similar samples were prepared to measure the evolution of H_2 gas during the degradation of the samples in PBS with a test area of 0.283 cm^2 using an eudiometer and based on the methodology presented in ref 32. For surface morphology assessment, the samples were ultrasonically washed with distilled water for 5 min to remove the salty crystals deposited on the surface from the PBS solution. Scanning electron microscopy (SEM) imaging and energy-dispersive X-ray (EDX) spectroscopy were used to assess the surface morphology and

DOI: 10.1021/acsomega.9b02976
ACS Omega 2019, 4, 21931−21944

chemical composition of the samples, respectively. Three samples were tested for each interval.

4.7. In Vitro Biological Tests. *4.7.1. Osteoblast Cell Morphological Analysis.* To study the in vitro osteocompatibility of the coated samples, the cell morphology, adhesion, and proliferation of the MC3T3-E1 osteoblast cell line (Sigma-Aldrich) on the coated samples were monitored. A suspension of 8×10^3 cells in 1× Dulbecco's modified Eagle's medium (DMEM) supplemented with 10% fetal bovine serum as well as 1% pericyte growth supplement was seeded on the surfaces of the samples, which were held under 5% CO_2 at 37 °C. After the samples were cultured for 3 days, the culture medium was extracted, and all of the samples were washed with PBS, fixed with 3% glutaraldehyde for 30 min, and then washed again 3 times with PBS. Next, the samples were dehydrated according to previous protocols.[53] Finally, the morphology of the cells was observed using SEM (JEOL 7001F, Japan).

4.7.2. Direct Cytotoxicity Assessment. Three timelines (6, 12, and 24 h) were used, and 1.6×10^4 MC3T3-E1 cells were directly seeded on the samples.[32] The 3-(4,5-dimethylthiazol-2-yl)-2,5-diphenyltetrazolium bromide (MTT, Sigma-Aldrich, Australia) assay was conducted to assess the cytotoxicity.[54] Briefly, after cell seeding, the samples were kept in the incubator at 37 °C and 5% CO_2. Then, 15 μL of the MTT solution with a concentration of 5 mg mL^{-1} was added to each well and incubated at 37 °C and 5% CO_2 for 4 h. Next, 150 μL of dimethyl sulfoxide (DMSO, Fisher Scientific, U.K.) was added to each well and incubated at room temperature for 10 min. Finally, a microplate reader (Benchmark Plus, Bio-Rad) at 570 nm was applied to measure the absorbance. Simultaneously with the cell culture experiments, parallel samples were prepared to measure the pH value of the culture medium using a pH meter (Thermo Fisher Scientific) to investigate the change in pH with time.

4.7.3. Indirect Viability Assessment. The MTT assay similar to that described in Section 4.7.2 was conducted to assess the cell viability. Each sample was first soaked in 150 μL of the prepared culture medium for 24 h at 37 °C and 5% CO_2. Then, the extracted media were diluted with 1× DMEM to a 1:1 ratio and used for subsequent experiments, including fixed-cell confocal imaging and viability assessment. For confocal imaging, 1.6×10^4 MC3T3-E1 cells were seeded on a round coverslip slide. At the same time, 8×10^3 MC3T3-E1 cells were seeded on a 96-well plate. Three wells were used per group for each experiment. Fresh media were used as the control groups in both experiments. The cells were cultured for 1 and 3 days at 37 °C and 5% CO_2. At the end of each timeline, the viability of each group of samples was assessed, and the absorbance was measured using the procedure described in Section 4.7.2.

To investigate the cytoskeletal arrangement of the cells using multiphoton confocal microscopy, similar samples in different groups were prepared using the fixation protocol presented by Guo et al.[55] and Marchesano et al.[56] Briefly, at the end of each time point, the culture medium was extracted and the MC3T3-E1 cells were washed with 1× PBS and fixed with 4% paraformaldehyde. Next, 0.1% Triton-X was added to permeabilize the cells (1 h). Then, the cells were kept in tetramethylrhodamine (TRITC)-conjugated phalloidin for 1 h. Finally, the cell nuclei were stained by incubation in 4′,6-diamidino-2-phenylindole for 10 min at room temperature.

4.8. In Vivo Animal Tests. A total of 10 albino rats of the Wistar strain with initial weights of 350−375 g were used in the present work. Each rat was kept and housed in a separate cage and fed with a standard diet and water. All animal procedures including animal selection, preparation, and surgical protocol were conducted based on protocols approved by the local ethical committee and laboratory animal administration rules of China.

4.8.1. Study Design. On the basis of the results of the material characterization and in vitro experiments, an in vivo animal study was designed to investigate the effect of the Mg−phenolic network coatings on the corrosion resistance and biocompatibility of Mg-based implants using the rat calvarial model. Two critical-sized defects each 5 mm in diameter were created in the parietal bone of each rat calvarium. One defect was used as the sham group, and a Mg disk was implanted on the other. Two types of Mg disks were used: uncoated (raw) and coated with Mg−phenolic networks at a Mg concentration of 3.6 mg mL^{-1}. Five rats were allocated to each of the two Mg implant groups for 4 weeks of observation after surgery.

4.8.2. Surgical Procedure. The surgical procedure was based on the steps mentioned in refs 48 and 57. The surgical procedure was based on the steps mentioned in refs 40 and 41. Briefly, the rats were sedated in a chamber with 4% isoflurane in 100% O_2 and then anesthetized by intraperitoneal injection of 15 mg kg^{-1} Zoletile and 10 mg kg^{-1} Rompun. Under local anesthesia with 2% lidocaine hydrochloride containing 1:100 000 epinephrine, after disinfection with povidone iodine, a middle skin incision was made on a shaved skin area on the skull and a full-thickness flap was reflected. Under copious saline irrigation, two standardized round defects each 5 mm in diameter were created on the left and right lateral parietal bones of the rat skull using a trephine bur. After the two critical-size calvarial bone defects, a Mg disk with a diameter of 5 mm and thickness of 0.8 mm was implanted in the right defect and the left defect was used as the sham group. Then, the periosteum and shaved skin were repositioned and sutured properly. After a healing period of 4 weeks, five rats in each group were euthanized in a CO_2 chamber. Subsequently, block sections of the rat skull will were collected and fixed in a 4% paraformaldehyde solution.

4.8.3. Observation of Subcutaneous Hydrogen Gas Cavity. Photographs of hydrogen gas accumulation in the implantation area of the Mg disk and any subcutaneous hydrogen gas cavities that formed within 4 weeks after implantation were obtained before the animals were harvested.

4.8.4. Micro-CT Analysis. A micro-computed tomography (μCT) scanner was chosen (μCT 40, Scanco Medical, Brüttisellen, Switzerland) to assess the harvested and fixed rats' cranial bone blocks at an isotropic voxel size of 18 μm. The X-ray source voltage and current were controlled at 90 kV and 110 μA, respectively. Finally, the images were reconstructed and processed using CTVox volume rendering software (Bruker).

4.9. Statistical Analysis. Statistical analyses were performed via one-way analysis of variance (ANOVA) using SigmaPlot ver13.0 (Systat Software, Inc.) software package.

■ ASSOCIATED CONTENT

Supporting Information

The Supporting Information is available free of charge at https://pubs.acs.org/doi/10.1021/acsomega.9b02976.

Effect of the coating cycle on the surface morphology of the coated samples (PDF)

DOI: 10.1021/acsomega.9b02976
ACS Omega 2019, 4, 21931−21944

AUTHOR INFORMATION

Corresponding Authors

*E-mail: yin.xiao@qut.edu.au. Tel: +61-7-31386240. Fax: +61-7-31386030 (Y.X.).
*E-mail: zhiyong.li@qut.edu.au. Tel: +61-7-31385112 (Z.L.).

ORCID

Mohammad Asgari: 0000-0002-6358-3624
Prasad K. D. V. Yarlagadda: 0000-0002-7026-4795
Zhiyong Li: 0000-0002-6814-9165

Notes

The authors declare no competing financial interest.

ACKNOWLEDGMENTS

The authors gratefully acknowledge financial support from the Australian Research Council (ARC) (FT140101152). We thank Dr. Geoffrey Will for useful discussions in sample preparation and using his lab for conducting electrochemical tests.

REFERENCES

(1) Seitz, J.-M.; Durisin, M.; Goldman, J.; Drelich, J. W. Recent Advances in Biodegradable Metals for Medical Sutures: A Critical Review. *Adv. Healthcare Mater.* **2015**, *4*, 1915−1936.

(2) Asgari, M.; Hang, R.; Wang, C.; Yu, Z.; Li, Z.; Xiao, Y. Biodegradable Metallic Wires in Dental and Orthopedic Applications: A Review. *Metals* **2018**, *8*, 212−244.

(3) Wang, C.; Yang, H. T.; Li, X.; Zheng, Y. F. In Vitro Evaluation of the Feasibility of Commercial Zn Alloys as Biodegradable Metals. *J. Mater. Sci. Technol.* **2016**, *32*, 909−918.

(4) Chen, Y.; Zhang, W.; Maitz, M. F.; Chen, M.; Zhang, H.; Mao, J.; Zhao, Y.; Huang, N.; Wan, G. Comparative corrosion behavior of Zn with Fe and Mg in the course of immersion degradation in phosphate buffered saline. *Corros. Sci.* **2016**, *111*, 541−555.

(5) Li, H. F.; Xie, X. H.; Zheng, Y. F.; Cong, Y.; Zhou, F. Y.; Qiu, K. J.; Wang, X.; Chen, S. H.; Huang, L.; Tian, L.; Qin, L. Development of biodegradable Zn-1X binary alloys with nutrient alloying elements Mg, Ca and Sr. *Sci. Rep.* **2015**, *5*, No. 10719.

(6) Persaud-Sharma, D.; McGoron, A. Biodegradable Magnesium Alloys: A Review of Material Development and Applications. *J. Biomimetics, Biomater., Tissue Eng.* **2012**, *12*, 25−39.

(7) Wu, L.; Feyerabend, F.; Schilling, A. F.; Willumeit-Römer, R.; Luthringer, B. J. Effects of extracellular magnesium extract on the proliferation and differentiation of human osteoblasts and osteoclasts in coculture. *Acta Biomater.* **2015**, *27*, 294−304.

(8) Chen, Y.; Xu, Z.; Smith, C.; Sankar, J. Recent advances on the development of magnesium alloys for biodegradable implants. *Acta Biomater.* **2014**, *10*, 4561−4573.

(9) Pilarska, A. A.; Klapiszewski, Ł.; Jesionowski, T. Recent development in the synthesis, modification and application of Mg(OH)2 and MgO: A review. *Powder Technol.* **2017**, *319*, 373−407.

(10) Janning, C.; Willbold, E.; Vogt, C.; Nellesen, J.; Meyer-Lindenberg, A.; Windhagen, H.; Thorey, F.; Witte, F. Magnesium hydroxide temporarily enhancing osteoblast activity and decreasing the osteoclast number in peri-implant bone remodelling. *Acta Biomater.* **2010**, *6*, 1861−1868.

(11) Weizbauer, A.; Kieke, M.; Rahim, M. I.; Angrisani, G. L.; Willbold, E.; Diekmann, J.; Flörkemeier, T.; Windhagen, H.; Müller, P. P.; Behrens, P.; Budde, S. Magnesium-containing layered double hydroxides as orthopaedic implant coating materials—An in vitro and in vivo study. *J. Biomed. Mater. Res., Part B* **2016**, *104*, 525−531.

(12) Guo, M.; Muhammad, F.; Wang, A.; Qi, W.; Wang, N.; Guo, Y.; Wei, Y.; Zhu, G. Magnesium hydroxide nanoplates: a pH-responsive platform for hydrophobic anticancer drug delivery. *J. Mater. Chem. B* **2013**, *1*, 5273−5278.

(13) Haynes, W. M. *CRC Handbook of Chemistry and Physics*; CRC Press, 2014.

(14) Dorozhkin, S. V. Calcium orthophosphate coatings on magnesium and its biodegradable alloys. *Acta Biomater.* **2014**, *10*, 2919−2934.

(15) Harandi, S. E.; Banerjee, P. C.; Easton, C. D.; Singh Raman, R. K. Influence of bovine serum albumin in Hanks' solution on the corrosion and stress corrosion cracking of a magnesium alloy. *Mater. Sci. Eng., C* **2017**, *80*, 335−345.

(16) Tang, J.; Wang, J.; Xie, X.; Zhang, P.; Lai, Y.; Li, Y.; Qin, L. Surface coating reduces degradation rate of magnesium alloy developed for orthopaedic applications. *J. Orthop. Transl.* **2013**, *1*, 41−48.

(17) Kraus, T.; Fischerauer, S. F.; Hänzi, A. C.; Uggowitzer, P. J.; Löffler, J. F.; Weinberg, A. M. Magnesium alloys for temporary implants in osteosynthesis: In vivo studies of their degradation and interaction with bone. *Acta Biomater.* **2012**, *8*, 1230−1238.

(18) Chen, Q.; Thouas, G. A. Metallic implant biomaterials. *Mater. Sci. Eng., R* **2015**, *87*, 1−57.

(19) Witte, F.; Hort, N.; Vogt, C.; Cohen, S.; Kainer, K. U.; Willumeit, R.; Feyerabend, F. Degradable biomaterials based on magnesium corrosion. *Curr. Opin. Solid State Mater. Sci.* **2008**, *12*, 63−72.

(20) Tang, H.; Gao, Y. Preparation and characterization of hydroxyapatite containing coating on AZ31 magnesium alloy by micro-arc oxidation. *J. Alloys Compd.* **2016**, *688*, 699−708.

(21) Zhao, N.; Zhu, D. Collagen Self-Assembly on Orthopedic Magnesium Biomaterials Surface and Subsequent Bone Cell Attachment. *PLoS One* **2014**, *9*, No. 110420.

(22) Wang, Z.-L.; Yan, Y.-H.; Wan, T.; Yang, H. Poly(L-lactic acid)/hydroxyapatite/collagen composite coatings on AZ31 magnesium alloy for biomedical application. *Proc. Inst. Mech. Eng., Part H* **2013**, *227*, 1094−1103.

(23) Xiong, P.; Yan, J.; Wang, P.; Jia, Z.; Zhou, W.; Yuan, W.; Li, Y.; Liu, Y.; Cheng, Y.; Chen, D.; Zheng, Y. A pH-sensitive self-healing coating for biodegradable magnesium implants. *Acta Biomater.* **2019**, *98*, 160−173.

(24) Wang, C.; Fang, H.; Qi, X.; Hang, C.; Sun, Y.; Peng, Z.; Wei, W.; Wang, Y. Silk fibroin film-coated MgZnCa alloy with enhanced in vitro and in vivo performance prepared using surface activation. *Acta Biomater.* **2019**, *91*, 99−111.

(25) Stippich, F.; Vera, E.; Wolf, G. K.; Berg, G.; Friedrich, C. Enhanced corrosion protection of magnesium oxide coatings on magnesium deposited by ion beam-assisted evaporation. *Surf. Coat. Technol.* **1998**, *103−104*, 29−35.

(26) Abela, I. S. Physical Vapour Deposition on Mg Alloys for Biomedical Applications. In *Surface Modification of Magnesium and Its Alloys for Biomedical Applications*; Narayanan, T. S. N. S., Park, I.-S., Lee, M.-H., Eds.; Woodhead Publishing, 2015; Chapter 4, pp 81−100.

(27) Cipriano, A. F.; Lin, J.; Miller, C.; Lin, A.; Cortez Alcaraz, M. C.; Soria, P.; Liu, H. Anodization of magnesium for biomedical applications − Processing, characterization, degradation and cytocompatibility. *Acta Biomater.* **2017**, *62*, 397−417.

(28) Kotoka, R.; Worthy, A.; Clinard, E.; Pai, D.; Sankar, J.; Yarmolenko, S. In *Application of Magnesium Oxide Functional Coating for Controlling the Corrosion of Magnesium for Implant Applications*, ASME 2012 International Mechanical Engineering Congress and Exposition, Nov 9, 2012; pp 731−735.

(29) Ejima, H.; Richardson, J. J.; Caruso, F. Metal-phenolic networks as a versatile platform to engineer nanomaterials and biointerfaces. *Nano Today* **2017**, *12*, 136−148.

(30) Yang, L.; Han, L.; Ren, J.; Wei, H.; Jia, L. Coating process and stability of metal-polyphenol film. *Colloids Surf., A* **2015**, *484*, 197−205.

(31) Rahim, M. A.; Björnmalm, M.; Bertleff-Zieschang, N.; Besford, Q.; Mettu, S.; Suma, T.; Faria, M.; Caruso, F. Rust-Mediated Continuous Assembly of Metal−Phenolic Networks. *Adv. Mater.* **2017**, *29*, No. 1606717.

(32) Chen, Y.; Zhao, S.; Liu, B.; Chen, M.; Mao, J.; He, H.; Zhao, Y.; Huang, N.; Wan, G. Corrosion-Controlling and Osteo-Compatible Mg Ion-Integrated Phytic Acid (Mg-PA) Coating on Magnesium Substrate for Biodegradable Implants Application. *ACS Appl. Mater. Interfaces* **2014**, *6*, 19531−19543.

DOI: 10.1021/acsomega.9b02976
ACS Omega 2019, 4, 21931−21944

(33) Chen, Y.; Zhang, X.; Zhao, S.; Maitz, M. F.; Zhang, W.; Yang, S.; Mao, J.; Huang, N.; Wan, G. In situ incorporation of heparin/bivalirudin into a phytic acid coating on biodegradable magnesium with improved anticorrosion and biocompatible properties. *J. Mater. Chem. B* **2017**, *5*, 4162−4176.
(34) Sun, J.; Zhu, Y.; Meng, L.; Chen, P.; Shi, T.; Liu, X.; Zheng, Y. Electrophoretic deposition of colloidal particles on Mg with cytocompatibility, antibacterial performance, and corrosion resistance. *Acta Biomater.* **2016**, *45*, 387−398.
(35) Webb, K.; Hlady, V.; Tresco, P. A. Relative importance of surface wettability and charged functional groups on NIH 3T3 fibroblast attachment, spreading, and cytoskeletal organization. *J. Biomed. Mater. Res.* **1998**, *41*, 422−430.
(36) Rodriguez-Contreras, A.; Guadarrama Bello, D.; Flynn, S.; Variola, F.; Wuest, J. D.; Nanci, A. Chemical nanocavitation of surfaces to enhance the utility of stainless steel as a medical material. *Colloids Surf., B* **2018**, *161*, 677−687.
(37) Janssen, M. I.; van Leeuwen, M. B. M.; van Kooten, T. G.; de Vries, J.; Dijkhuizen, L.; Wösten, H. A. B. Promotion of fibroblast activity by coating with hydrophobins in the β-sheet end state. *Biomaterials* **2004**, *25*, 2731−2739.
(38) Rosales-Leal, J. I.; Rodríguez-Valverde, M. A.; Mazzaglia, G.; Ramón-Torregrosa, P. J.; Díaz-Rodríguez, L.; García-Martínez, O.; Vallecillo-Capilla, M.; Ruiz, C.; Cabrerizo-Vílchez, M. A. Effect of roughness, wettability and morphology of engineered titanium surfaces on osteoblast-like cell adhesion. *Colloids Surf., A* **2010**, *365*, 222−229.
(39) GaweL, L.; Nieuzyla, L.; Nawrat, G.; Darowicki, K.; Slepski, P. Impedance monitoring of corrosion degradation of plasma electrolytic oxidation coatings (PEO) on magnesium alloy. *J. Alloys Compd.* **2017**, *722*, 406−413.
(40) Banerjee, C. P.; Woo, P. R.; Grayson, M. S.; Majumder, A.; Raman, K. R. Influence of Zeolite Coating on the Corrosion Resistance of AZ91D Magnesium Alloy. *Materials* **2014**, *7*, 6092−6104.
(41) Sherif, E.-S. M. Corrosion behavior of magnesium in naturally aerated stagnant seawater and 3.5% sodium chloride solutions. *Int. J. Electrochem. Sci.* **2012**, *7*, 4235−4249.
(42) Ren, Y.; Babaie, E.; Lin, B.; Bhaduri, S. B. Microwave-assisted magnesium phosphate coating on the AZ31 magnesium alloy. *Biomed. Mater.* **2017**, *12*, No. 045026.
(43) Gonzalez, J.; Hou, R. Q.; Nidadavolu, E. P. S.; Willumeit-Römer, R.; Feyerabend, F. Magnesium degradation under physiological conditions − Best practice. *Bioact. Mater.* **2018**, *3*, 174−185.
(44) Kokubo, T.; Takadama, H. How useful is SBF in predicting in vivo bone bioactivity? *Biomaterials* **2006**, *27*, 2907−2915.
(45) Galow, A.-M.; Rebl, A.; Koczan, D.; Gimsa, J. MC3T3 osteoblast-like cells cultured at alkaline pH: Microarray data (Affymetrix GeneChip Mouse 2.0 ST). *Data Brief* **2017**, *13*, 108−114.
(46) Galow, A.-M.; Rebl, A.; Koczan, D.; Bonk, S. M.; Baumann, W.; Gimsa, J. Increased osteoblast viability at alkaline pH in vitro provides a new perspective on bone regeneration. *Biochem. Biophys. Rep.* **2017**, *10*, 17−25.
(47) Shen, Y.; Liu, W.; Wen, C.; Pan, H.; Wang, T.; Darvell, B. W.; Lu, W. W.; Huang, W. Bone regeneration: importance of local pH—strontium-doped borosilicate scaffold. *J. Mater. Chem.* **2012**, *22*, 8662−8670.
(48) Lin, D.-J.; Hung, F.-Y.; Lee, H.-P.; Yeh, M.-L. Development of a novel degradation-controlled magnesium-based regeneration membrane for future guided bone regeneration (GBR) therapy. *Metals* **2017**, *7*, 481−498.
(49) Cui, W.; Beniash, E.; Gawalt, E.; Xu, Z.; Sfeir, C. Biomimetic coating of magnesium alloy for enhanced corrosion resistance and calcium phosphate deposition. *Acta Biomater.* **2013**, *9*, 8650−8659.
(50) Narayanan, T. S.; Park, I.-S.; Lee, M.-H. *Surface Modification of Magnesium and Its Alloys for Biomedical Applications: Modification and Coating Techniques*; Elsevier, 2015.
(51) Makkar, P.; Sarkar, S. K.; Padalhin, A. R.; Moon, B.-G.; Lee, Y. S.; Lee, B. T. In vitro and in vivo assessment of biomedical Mg−Ca alloys for bone implant applications. *J. Appl. Biomater. Funct. Mater.* **2018**, *16*, 126−136.
(52) Wang, Q.; Tan, L.; Xu, W.; Zhang, B.; Yang, K. Dynamic behaviors of a Ca−P coated AZ31B magnesium alloy during in vitro and in vivo degradations. *Mater. Sci. Eng., B* **2011**, *176*, 1718−1726.
(53) Cheng, J.; Liu, B.; Wu, Y. H.; Zheng, Y. F. Comparative in vitro Study on Pure Metals (Fe, Mn, Mg, Zn and W) as Biodegradable Metals. *J. Mater. Sci. Technol.* **2013**, *29*, 619−627.
(54) He, L. Y.; Zhang, X. M.; Liu, B.; Tian, Y.; Ma, W. H. Effect of magnesium ion on human osteoblast activity. *Braz. J. Med. Biol. Res.* **2016**, *49*, 5257−5263.
(55) Guo, Y.; Hu, B.; Tang, C.; Wu, Y.; Sun, P.; Zhang, X.; Jia, Y. Increased osteoblast function in vitro and in vivo through surface nanostructuring by ultrasonic shot peening. *Int. J. Nanomed.* **2015**, *10*, 4593−4603.
(56) Marchesano, V.; Gennari, O.; Mecozzi, L.; Grilli, S.; Ferraro, P. Effects of lithium niobate polarization on cell adhesion and morphology. *ACS Appl. Mater. Interfaces* **2015**, *7*, 18113−18119.
(57) An, Y.-Z.; Heo, Y.-K.; Lee, J.-S.; Jung, U.-W.; Choi, S.-H. Dehydrothermally Cross-Linked Collagen Membrane with a Bone Graft Improves Bone Regeneration in a Rat Calvarial Defect Model. *Materials* **2017**, *10*, 927−939.

DOI: 10.1021/acsomega.9b02976
ACS Omega 2019, 4, 21931−21944